doi:10.1016/S0022-2836(02)00735-0 available online at http://www.idealibrary.com on IDEAL® J. Mol. Biol. (2002) 322, 1089–1102

JMB

α-Synuclein, Especially the Parkinson's Disease-associated Mutants, Forms Pore-like Annular and Tubular Protofibrils

Hilal A. Lashuel[1], Benjamin M. Petre[2], Joseph Wall[3], Martha Simon[3] Richard J. Nowak[1], Thomas Walz[2] and Peter T. Lansbury Jr[1]*

[1]*Center for Neurologic Diseases Brigham and Women's Hospital and Department of Neurology Harvard Medical School Partners Research Bldg 65 Landsdowne St., Room 451 Cambridge, MA 02139, USA*

[2]*Department of Cell Biology Harvard Medical School 240 Longwood Avenue Boston, MA 02115, USA*

[3]*Department of Biology Brookhaven National Laboratory, Building 463 Upton, NY 11973, USA*

**Corresponding author*

Two mutations in the α-synuclein gene (A30P and A53T) have been linked to autosomal dominant early-onset Parkinson's disease (PD). Both mutations promote the formation of transient protofibrils (prefibrillar oligomers), suggesting that protofibrils are linked to cytotoxicity. In this work, the effect of these mutations on the structure of α-synuclein oligomers was investigated using electron microscopy and digital image processing. The PD-linked mutations (A30P and A53T) were observed to affect both the morphology and the size distribution of α-synuclein protofibrils (measured by analytical ultracentrifugation and scanning transmission electron microscopy). The A30P variant was observed to promote the formation of annular, pore-like protofibrils, whereas A53T promotes formation of annular and tubular protofibrillar structures. Wild-type α-synuclein also formed annular protofibrils, but only after extended incubation. The formation of pore-like oligomeric structures may explain the membrane permeabilization activity of α-synuclein protofibrils. These structures may contribute to the pathogenesis of PD.

Keywords: α-synuclein; Parkinson's disease; protofibrils; transmission electron microscopy; scanning transmission electron microscopy

Introduction

Parkinson's disease (PD) is a neurodegenerative movement disorder that is characterized by the loss of dopaminergic neurons from the substantia nigra, and the formation of fibrillar intraneuronal inclusions (called Lewy bodies).[1–3] Several lines of evidence point towards a central role for the process of α-synuclein fibrillization in the etiology of PD. First, α-synuclein is the primary component of Lewy bodies in all PD patients[4]. Second, two different α-synuclein missense mutations (A30P and A53T) are associated with rare, autosomal dominant, early-onset PD[5,6] and have been shown to form fibrils. Third, transgenic mice and Drosophila expressing human wild-type (WT) α-synuclein or, in the flies, the mutants, are characterized by α-synuclein inclusions that resemble Lewy bodies.[7,8] In both models, the formation of these inclusions is correlated to the onset of disease phenotype. Finally, the PD-linked mutations (A30P and A53T), promote *in vitro* α-synuclein oligomerization,[9–12] suggesting that the process of α-synuclein fibrillization may initiate neurodegeneration. α-Synuclein amyloid fibril formation proceeds through a series of discrete oligomeric intermediates, referred to as protofibrils, that disappear upon fibril formation.[13] Although both PD-linked mutations accelerate the formation of α-synuclein protofibrils, the A30P mutation was shown to delay the formation of amyloid fibrils relative to WT, suggesting that α-synuclein protofibrils, rather than fibrils, may be the pathogenic species.[13] This hypothesis[14] is supported by the observation that α-synuclein deposits in the brains of the "symptomatic" transgenic mice are

Abbreviations used: PD, Parkinson's disease; PFs, protofibrils; AFM, atomic force microscopy; GF, gel filtration; AU, analytical ultracentrifugation; SVAU, sedimentation velocity analytical ultracentrifugation; EM, electron microscopy; STEM, scanning transmission electron microscopy; *M*, molecular mass; HM, high molecular mass; WT, wild-type human α-synuclein; PK, proteinase K.

E-mail address of the corresponding author: plansbury@rics.bwh.harvard.edu

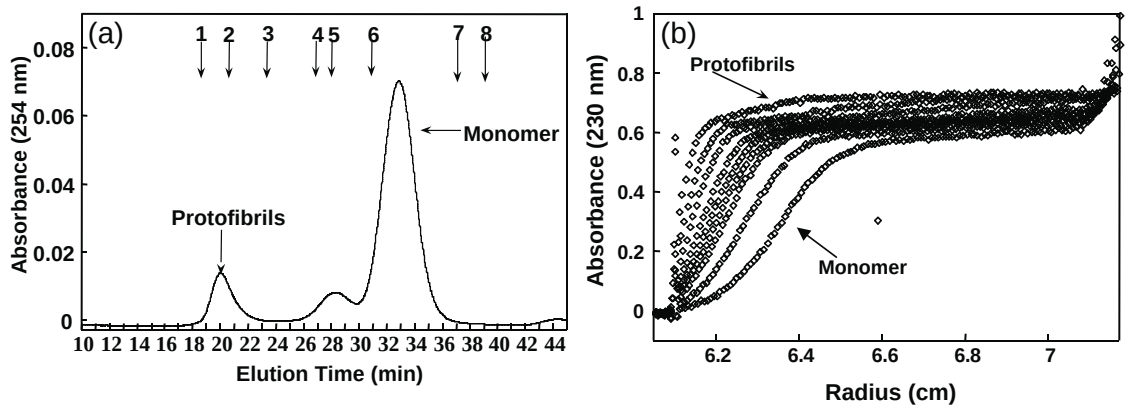

Figure 1. α-Synuclein forms protofibrils that can be resolved by GF and SVAU methods. (a) An analytical GF chromatogram of α-synuclein (A53T) stock solution (350 μM). α-Synuclein in 10 mM Tris–HCl (pH 7.4), 150 mM NaCl was loaded onto a Superdex 200 HR 10/30 GF column, and elution of the protein was followed by measuring absorbance at 220 nm and at 254 nm. The arrows indicate the elution volumes of the standards (blue dextran 2000 (1), thyroglobulin, 669 kDa (2); ferritin, 440 kDa (3); catalase, 232 kDa (4); aldolase, 158 kDa (5); albumin, 68 kDa (6); chymotrypsinogen A, 25 kDa (7); and ribonuclease A, 13.7 kDa (8)). (b) Sedimentation velocity profiles of A53T stock solution (200 μM). The fast-sedimenting boundary (arrow) corresponds to the sedimentation of A53T protofibrils, whereas the slowly sedimenting boundary corresponds to the sedimentation of predominantly monomeric A53T.

non-fibrillar,[7] and the fact that dopaminergic neurons that contain Lewy bodies appear to be healthier than neighboring neurons.[2,15]

Atomic force microscopy (AFM) analysis of α-synuclein oligomerization demonstrates that α-synuclein protofibrils exist in spherical, chain-like and annular morphologies.[11,13,16,17] Here, we investigated the effect of the familial PD mutations on the structural properties of α-synuclein protofibrils. By extending the biophysical studies to electron microscopy (EM), analytical ultracentrifugation (AU) and scanning transmission electron microscopy (STEM), we show that protofibrils of defined molecular size distribution and morphology are formed. In addition, we present a detailed analysis of the morphological types of protofibrils using EM and single-particle averaging of negatively stained specimens. The potential relevance of the observed structures to the mechanism of pathogenesis of PD is discussed.

Results

α-Synuclein protofibrils are metastable and can be separated and quantified by gel filtration and sedimentation velocity

At concentrations of ≥200 μM in PBS (pH 7.4), α-synuclein forms prefibrillar oligomeric species, known as protofibrils, which disappear upon formation of amyloid fibrils.[9,11,13] To examine the effect of α-synuclein mutations on the formation of protofibrils, we determined the amount of protofibrils formed by both the mouse and human α-synuclein (WT), and the human PD-linked mutants A30P and A53T by gel filtration (GF) (~350 μM) using a Superdex 200 HR column. The relative amount of protofibrils was determined by calculating the area under the void peak using the Millenium software (Waters, Milford, MA). Figure 1(a) shows a typical GF chromatogram of A53T α-synuclein. α-Synuclein eluted as three peaks corresponding to protofibrillar oligomeric species (20 minutes), dimer† (28 minutes), and monomer (33 minutes). Protofibrils were observed with the four protein variants. The relative amounts of protofibrils formed under identical solution conditions were as follows: mouse > A53T > A30P > human WT α-synuclein (data not shown). The amount of protofibrils formed never exceeded 15% of the total protein in solution. After reaching a critical concentration,[13] protofibrils suddenly disappeared, coincident with the appearance of amyloid fibrils (as observed in the EM). Analysis of α-synuclein protofibril fractions by matrix-assisted laser desorption ionization (MALDI) mass spectrometry revealed a single molecular mass value identical with that of full-length α-synuclein (Supplementary Material Figure 1).

The homogeneity of the stock solutions analyzed by GF was assessed by sedimentation velocity analytical ultracentrifugation (SVAU). Sedimentation velocity studies revealed that α-synuclein (200 μM) sedimented as two boundaries; a fast-moving boundary corresponding to protofibrils, and a slowly moving boundary corresponding to

† Analysis of this dimer by matrix-assisted laser desorption/ionization (MALDI) mass spectrometry and sedimentation velocity revealed an apparent mass of 28 kDa, consistent with a covalent dimer. Furthermore, incubation of monomeric α-synuclein (37 °C) revealed a steady increase in the void peak, but no dimer peak was observed by GF. It is unknown what the dimer represents, whether it is an artifact of bacterial expression or normal cells may secrete dimeric forms.

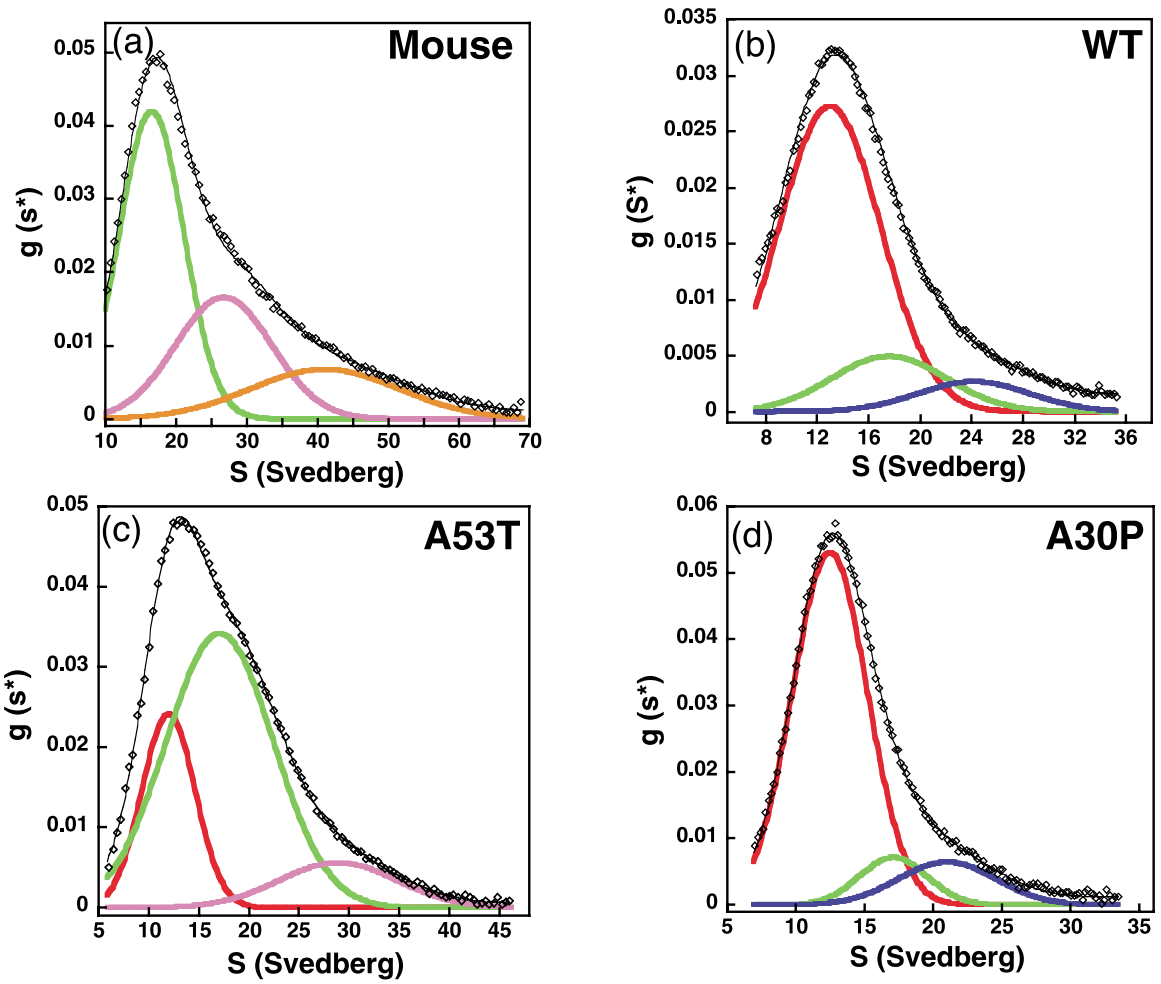

Figure 2. The distribution of protofibrillar quaternary structures is dependent on the variant of α-synuclein. The apparent distributions of sedimentation coefficient ($g(s^*)$) for (a) mouse WT, (b) human WT, (c) A53T and (d) A30P α-synuclein were obtained using time derivative analysis of the SVAU data for each protein at 300 μM. The black line reflects the best least-squares fit of the data (O) to a three-species model using a Gaussian function.

the monomer and dimer (Figure 1(b)). The amount of protofibrils formed (on the basis of absorbance values) corresponded to ≤10% of the total protein in solution, consistent with GF chromatography results. Furthermore, dilution and/or re-injection of purified protofibril fractions onto the GF column revealed only very small amounts of monomer, even after ten days of incubation at 4 °C (data not shown).

To estimate the molecular mass (M_r) of α-synuclein protofibrils, the retention time on Superdex 200 was compared to those of other proteins with sizes ranging from 13.7 kDa to 669 kDa (Figure 1(a)). The early void peak containing α-synuclein protofibrils eluted slightly ahead of thyroglobulin (669 kDa), whereas the middle fractions of the peak eluted between the thyroglobulin and ferritin (440 kDa) standards, suggesting an average M_r for the protofibrils of greater than 600 kDa (corresponding to >42 monomers). However, α-synuclein monomer and dimer,[1] identified by SVAU analysis, eluted with an apparent M_r of 67 kDa (33 minutes) and 125 kDa (28 minutes), suggesting a non-globular shape for both forms. Accordingly, a non-globular conformation of α-synuclein would result in an overestimation of M_r for protofibrils.

AU of the heterogeneous protofibril fraction reveals four subpopulations, the occupancy of which is sensitive to the mutations

To estimate the size distribution of protofibrillar structures and to characterize their morphology, SVAU and EM analyses were performed. Protofibrils of mouse, human WT, A30P, and A53T (5 mg/ml) were fractionated and analyzed. The sedimentation profiles were analyzed using the time derivative method to yield the apparent distribution of sedimentation coefficients, $g(s^*)$. Figure 2 shows the distributions of sedimentation coefficients obtained from experiments performed on purified protofibrils of the four variants. The prominent maximum corresponds to the sedimentation coefficient of the major species in solution. When compared to human α-synuclein variants, mouse α-synuclein showed a broader distribution of sedimenting species (10–70 S), suggesting that

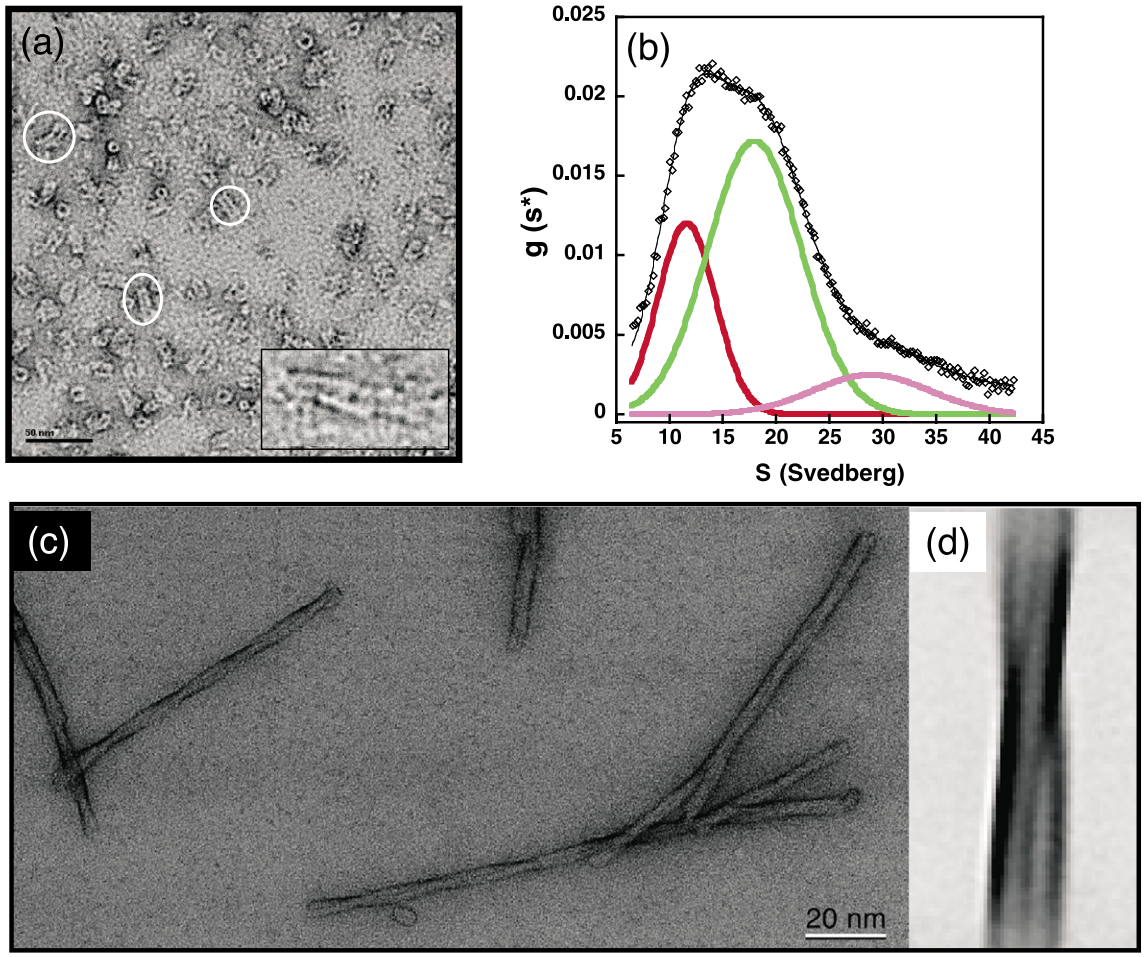

Figure 3. Time-dependent EM and SVAU reveals a shift in molecular mass distribution and conversion of annular particles into tubular structures. (a) Electron micrograph area of negatively stained A53T protofibrils incubated at 4 °C for one month. (b) The apparent distribution of sedimentation coefficients of purified A53T protofibrils after incubation at 4 °C for 12 days. (c) Typical electron micrograph area taken from a negatively stained A30P fibril formed from A30P protofibrils in the presence of monomeric α-synuclein. (d) Projection average of an A30P fibril calculated from 549 cut-out fibril crossovers.

this protein formed oligomers of greater molecular mass. In addition to the 17 S population (green line) being the major species in solution, the $g(s^*)$ plot revealed two other sub-populations of protofibrils with average sedimentation coefficients of 28 S (pink) and 42 S (orange) (Figure 2(a)). Human WT oligomers showed a narrower distribution of species, the major one having a sedimentation coefficient of 13 S (red line, Figure 2(b)). Like mouse α-synuclein, the A53T protofibrils were dominated by the 17 S species (Figure 2(c)). In contrast, the A30P variant protofibrils exhibited a distribution similar to that of human WT α-synuclein (Figure 2(d)). In negatively stained EM samples, the protofibrils showed a heterogeneous distribution of morphologies. In addition to the spherical protofibrils, significant amounts of novel annular and tubular protofibrils of identical diameters (~11(±1) nm) were observed in the case of the PD-linked variants sample (see below). Although the WT oligomers showed a sedimentation coefficient distribution similar to that of the A30P variant (the major species having a sedimentation coefficient of 13 S), examination by EM revealed the absence of annular and tubular protofibrils.

Over time, annular protofibrils form tubes, then ultimately fibrils

To investigate whether the annular and tubular protofibrils represent different stages of assembly into amyloid fibrils, we carried out time-dependent EM and SVAU studies on WT, A53T, and A30P α-synuclein protofibrils. Although the protofibrils retained the annular and tubular morphologies even after incubation for one to two months at 4 °C, over time, their size distribution shifted towards higher M_r protofibrillar structures (Figure 3(a)). For example, SVAU experiments on purified A53T protofibrils after 12 days of incubation (4 °C) demonstrated a significant increase in the amount of the 17 S species in solution, suggesting a slow conversion between the species in solution (compare Figure 3(b) to Figure 2(c)). In contrast, the apparent sedimentation coefficient distribution

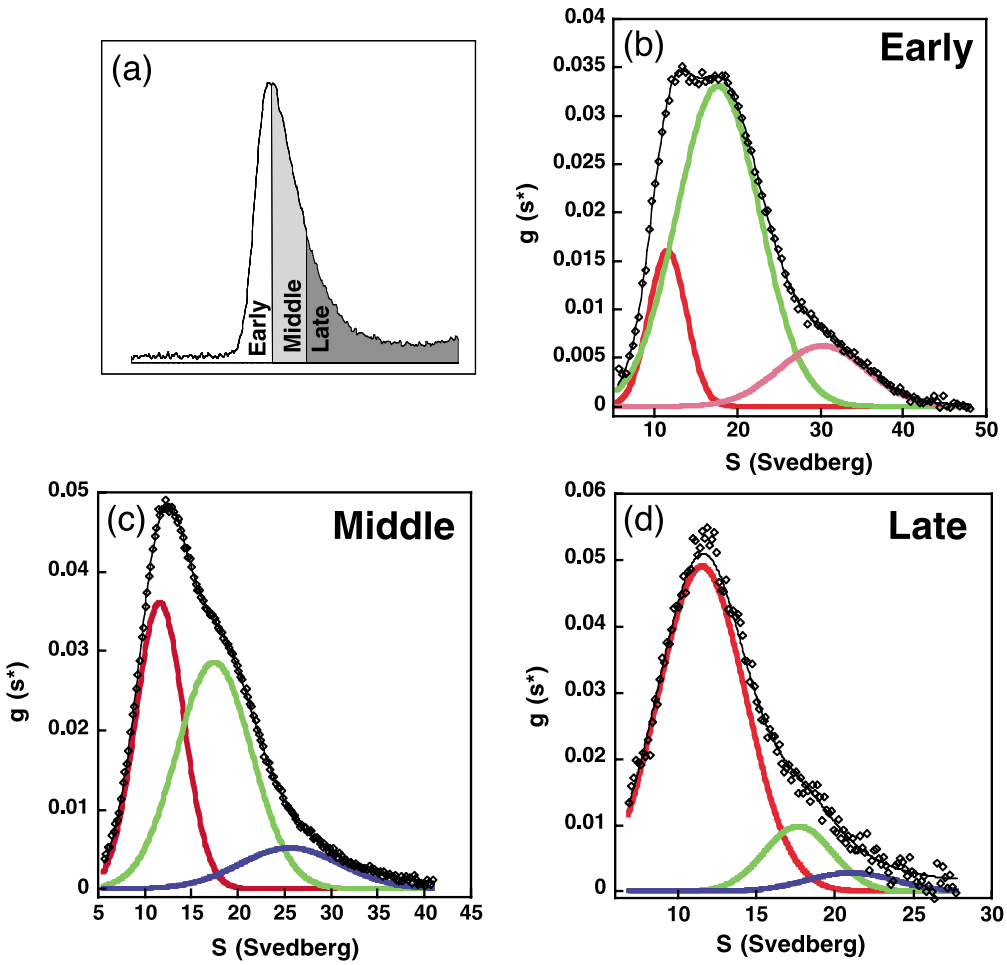

Figure 4. Relative separation of α-synuclein protofibrillar species by fractionation of the void protofibril peak. (a) Gel-filtration chromatogram illustrating how the void peak was divided into three fractions (early, middle, and late). The apparent distribution of sedimentation coefficients ($g(s^*)$) for the purified (b) early, (c) middle, and (d) late fractions of the void peak of A53T.

$g(s^*)$ of WT and A30P remained virtually unchanged over this time (data not shown). Negatively stained EM samples of A53T protofibrils incubated for two weeks (4 °C) also showed the presence of long tubular structures, which were absent at early time-points (Figure 3(a)). The observation of longer tubes is consistent with the shift in A53T molecular size distribution observed by SVAU. After four weeks of incubation at 4 °C, WT α-synuclein was observed to form annular protofibrils (Supplementary Material Figure 2), whereas spherical protofibrils ranging in diameter from 13 nm to 17 nm were observed for A30P after longer incubations. In all cases, fibril formation was not detected in the protofibrillar samples (even after ten days of incubation at 37 °C). In contrast, incubation of α-synuclein protofibrils in the presence of excess monomeric α-synuclein resulted in fibril formation and protofibril consumption within a few days at 37 °C. The fibrils exhibited a helical twist and had a diameter similar to that of the annular and tubular protofibrils (11 nm on average) (Figure 3(c) and (d)). The annular and tubular protofibrils exhibited resistance to proteinase K (PK), suggesting that they represent ordered intermediates on the fibrillogenesis pathway. After two hours of digestion with PK, several low M_r proteolytic-resistant fragments could be seen, one of which persisted even after four hours of treatment (Supplementary Material Figure 3). Similar fragments have been observed for α-synuclein fibrils after digestion with PK.[18] These fragments were mapped to the hydrophobic region of α-synuclein known as the non-amyloid component (NAC) (residues 61–95), thought to be critical for α-synuclein fibrillization.[18]

Fractionation of the protofibrillar void peak results in partial separation of α-synuclein protofibrillar morphologies

The sedimentation coefficient distribution plots of WT, A53T and A30P α-synuclein revealed the presence of two major populations of protofibrils with an average sedimentation coefficient of 13 S and 17 S (Figure 2), suggesting common protofibrillar intermediates on the pathway to the fibril. To gain further insight into the structural features of these protofibrillar intermediates, we sought to further purify these species by fractionation of the

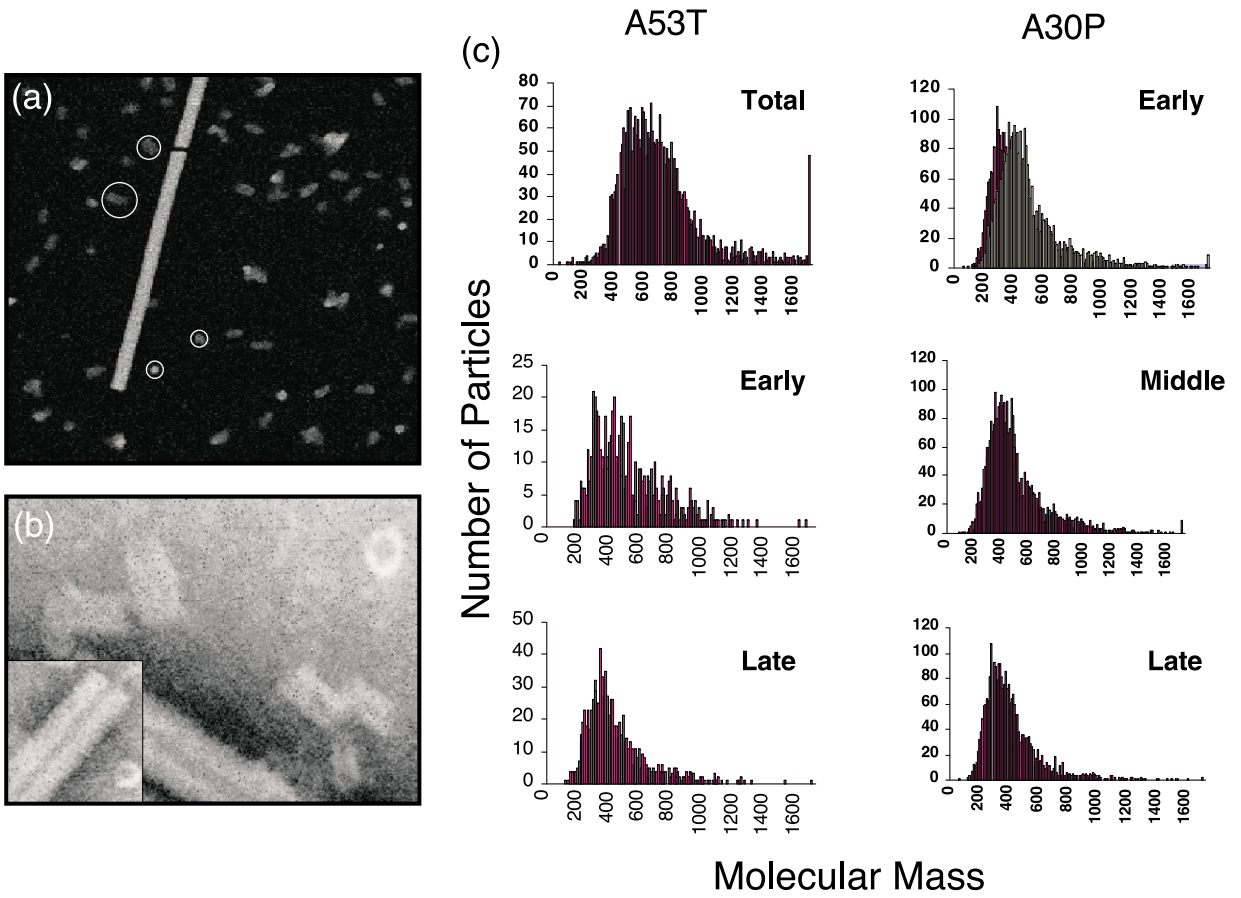

Figure 5. Quantitative STEM analysis of α-synuclein particles reveals a mass distribution consistent with that predicted by SVAU. (a) Electron micrograph of unstained/freeze-dried A53T-synuclein particles recorded by STEM. Light regions represent areas of high-mass density and dark regions represent areas of low mass density. (b) STEM micrographs of vanadate-stained protofibrillar fraction of A53T revealing annular and tubular structures. TMV (diameter 1.8 nm) was included in each specimen as an internal standard. (c) Histograms of molecular mass measurements of A53T and A30P particles from early, middle, and late protofibrillar void fractions purified by GF.

α-synuclein protofibril peak. Three fractions corresponding to the early, middle and late fractions of the void peak were collected using TSK-Gel G4000 SWxl GF column (Figure 4(a)). The fractions were concentrated to 15–20 μM prior to analysis. The sedimentation data again demonstrated the presence of three populations of protofibrils, with average sedimentation coefficients of 13(±1), 17(±1), and 25–30(±1) S (Figure 4(b)–(d)). Assuming a globular structure, these sedimentation coefficients correspond to an average M_r of 308 kDa ($n = 21$, $n =$ number of α-synuclein monomers), 368 kDa ($n = 26$), and 539 kDa ($n = 38$), respectively (see Materials and Methods). The early (fastest eluting) A53T fraction showed the 17 S as the major species followed by the 13 S and 30 S species (Figure 4(b)). The amount of the 13 S species increased in the late-eluting fraction (late, see Figure 4(a)), becoming the predominant species (Figure 4(c) and (d)). In the case of the A30P variant, the middle fraction consisted predominantly of the 13 S species, consistent with the narrow distribution observed by SVAU (Figure 2(d)). It is not clear whether the 13 S species corresponds to dissociated subunits of the higher species (17 S, 24 S or 40 S) or represents the first-formed protofibrillar species.

Quantitative analysis of α-synuclein protofibrillar subpopulations by STEM revealed a mass distribution consistent with that predicted by AUSV

STEM allows the determination of M_r of individual particles, independent of the shape or hydrodynamic properties of the particles. To correlate the M_r of A53T and A30P particles to a particular morphology, the various void peak fractions were analyzed by STEM. Protofibrils of various sizes could be distinguished on the images, and were selected automatically using a set of models of overlapping sizes (using the PCmass software), which located all isolated particles in each image. The predominant particle shapes observed were: (a) relatively amorphous round particles 13–15 nm in diameter; and (b) relatively compact particles roughly 9 nm in diameter, frequently with a central depression. The high brightness and central depression are consistent with a cylinder viewed end-on. Side-view tubes were observed

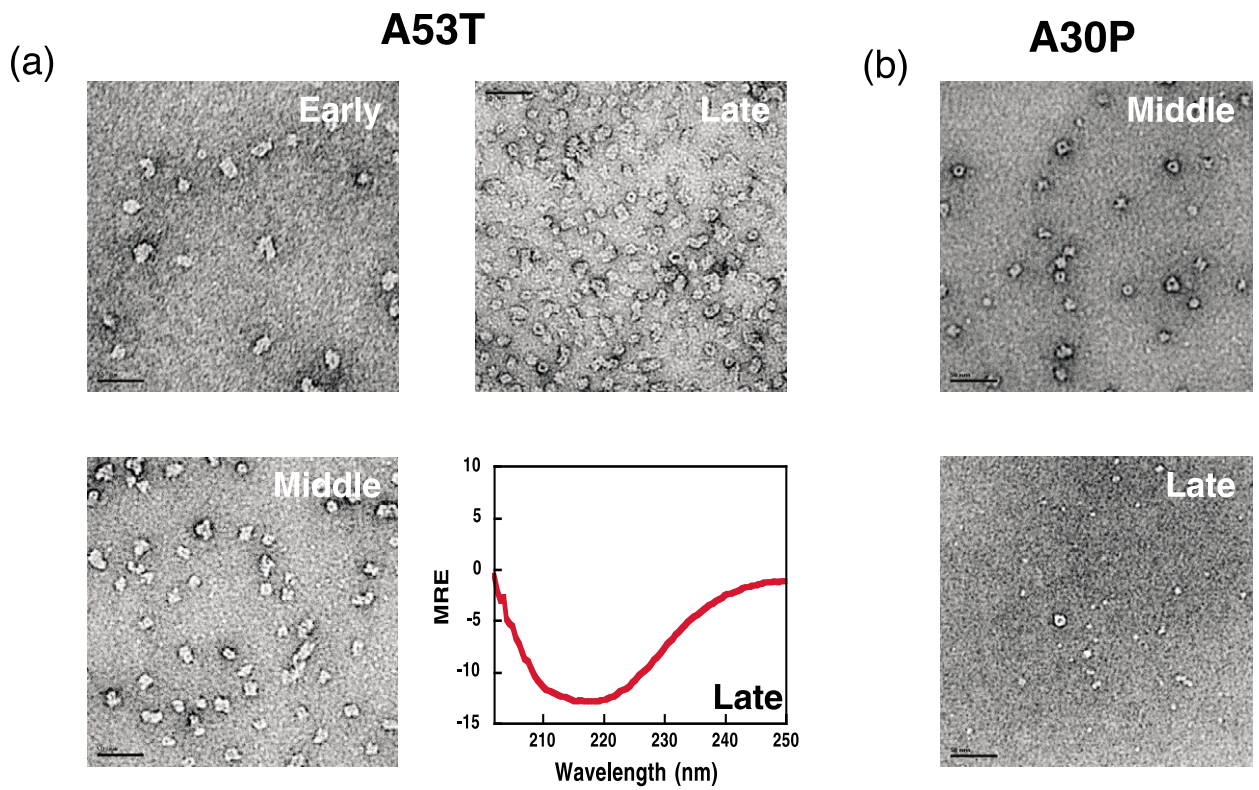

Figure 6. (a) Electron micrograph areas of negatively stained samples obtained from the fractionation of the A53T void peak. Far-UV CD spectrum of the late fraction demonstrating a high content of β-sheet for the A53T fraction (late) rich in annular protofibrils. (b) Electron micrograph areas of negatively stained samples obtained from the fractionation of the A30P void peak revealing annular and spherical protofibrils. The scale bars represent 50 nm.

frequently in the A53T void specimens (Figure 5(a) and (b)). Mass measurements of all detected particles demonstrated that partial separation of the protofibril populations was achieved by fractionation of the protofibril peak (Figure 5(c)). STEM analyses confirmed that A53T protofibrils are more heterogeneous and exhibit a wider molecular mass distribution relative to A30P (Figure 5(c)). An unfractionated sample of A53T protofibrils gave a mass distribution with a broad peak due to particles ranging in mass from 180 kDa to 950 kDa. Given a molecular mass of 14.4 kDa for the monomeric protein, this range would correspond to particles comprising 12–66 monomers. Interestingly, the late fractions yielded less heterogeneous protofibrils in the range of ~350(±50) kDa (24(±3) monomers), consistent with those predicted by SVAU (Figure 4(d)). For both A53T and A30P, there were very few particles in the 100 kDa range, consistent with the absence of any significant amount of sedimenting species with an *s* value below 10 S.

Differences in protofibril size distributions correspond to differences in protofibril morphology

Differences in the distribution of species detected by AU correspond to differences in protofibril morphology as examined by EM. For example, the early fraction of A53T contained predominantly large spherical and tubular species with an average diameter of 24 nm and 19 nm, respectively (Figure 6(a)). Occasionally, annular protofibrils with an average diameter of 11 nm could be seen in this fraction (Figure 6(a)). The amount of annular protofibrils increased significantly in the fraction corresponding to the middle of the A53T protofibril peak, whereas the majority of the species in the late fraction were 10–12 nm annular protofibrils (Figure 6(a)). The late fraction contained a significant amount of tubular species, which had an average diameter of 11 nm and an average length of 24 nm. The far-UV CD spectrum was consistent with a high content of β-sheet for the annular and tubular protofibrils.[19] The facts that the major protofibrillar species in this fraction is the 13 S species, and that the diameters of the annular and tubular protofibrils are very similar, suggest that the two morphologies may reflect top and side-views of the same hollow cylindrical protofibril structure. Alternatively, the annular species may represent the 13 S species (308 kDa), whereas the tubular structures may correspond to the 17 S species (368 kDa using equation (1), see Materials and Methods). For A30P, significant amounts of annular protofibrils were observed in both the early and middle fractions, but the middle fraction appeared to be more homogeneous (Figure 6(b)). The presence of spherical protofibrils was prominent in the late fraction of A30P (Figure 6(b)).

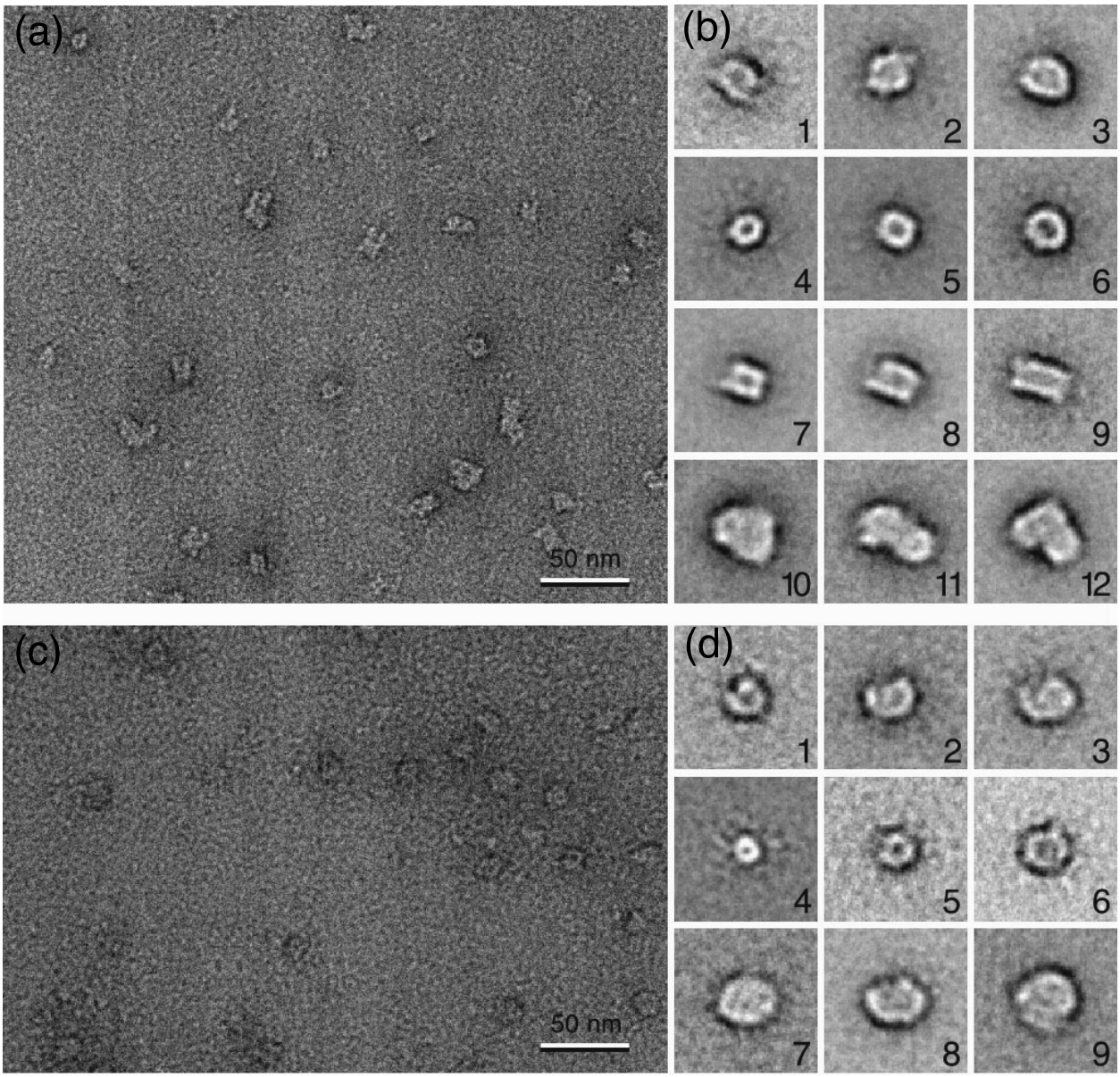

Figure 7. Electron microscopy and averaging of protofibrils reveal annular and tubular quaternary structures. (a) Negative stain EM of A53T protofibrils from the late fraction of the GF purified void peak. (b) A gallery of representative class averages calculated from a total of ~6000 A53T particles. (c) Negative stain EM of A30P protofibrils from the right fraction of the GF purified void peak. (d) A gallery of class averages calculated from a total of ~5000 A30P particles. The size of each box corresponds to 40.5 nm.

Single-particle averaging reveals a collection of distinct, yet related annular, helical, and tubular protofibrils

To gain further insight into the structural features of α-synuclein protofibrils, we analyzed protofibrillar fractions of A30P and A53T by negative stain EM and single-particle averaging. Electron micrographs of the late and middle fractions of the void peak for A53T and A30P showed annular and tubular structures with a relatively homogeneous size distribution, and were therefore chosen for further image processing. Representative images of negatively stained samples of A53T and A30P are shown in Figure 7(a) and (c). A total of 5000–6000 particles for each were selected from 31 images of A53T (late fraction) and from 16 images of A30P (middle fraction). Multivariate statistical analysis was then used to divide the data sets of 5815 particles for A53T and 5040 particles for A30P into 100 output classes (Supplementary Material Figure 4(a) and (b)). These 100 classes fell into four major groups of structures. A gallery with representative class averages obtained from images of A53T (late fraction) is shown in Figure 7(b), illustrating the four major groups of protofibril structures. The first group consisted of what appears to be incomplete rings, where one end of the protofibril seemed to lie above the other end, suggesting a

helical symmetry for these structures (Figure 7(b), 1–3). The second group showed annular structures having an average diameter of approximately 10–12 nm and a central stain-filled cavity that is 2 nm in diameter (Figure 7(b), 4–6). The third group showed rectangular particles with a mean diameter of 12 nm and varying length of 11–20 nm (Figure 7(b), 7–9). The presence of rectangular particles with similar diameter but closely spaced lengths is likely to reflect different stages of protofibrillar growth. The similar diameter observed for the annular and rectangular particles suggests that the two morphologies represent two different views (top and side-view) of the same species. Alternatively, the rectangular particles may form by end-to-end stacking of annular particles. The fourth group showed large aggregates, some of which appeared to be formed by two rectangular particles joint at a 90° angle (Figure 7(b), 10–12).

Figure 7(c) shows a typical area of an electron micrograph taken from negatively stained A30P (middle fraction), revealing the annular structures to be the predominant species in this sample. A gallery of representative averages of A30P (middle fraction) is shown in Figure 7(d), reflecting at least three groups of protofibrillar structures. The first group contained chain-like structures that formed rings with slightly displaced ends, which are likely to represent the precursors for the helical fibrils (Figure 7(d), 1–3). The second group represents the majority of the structures for A30P that consist of annular structures approximately 10–12 nm in diameter with an inner core diameter of 2–3 nm (Figure 7(d), 4–6). Rings of smaller diameter (~8 nm) were present in significant amounts. The third group contains large spherical particles with an average diameter of 24 nm (Figure 7(d), 7–9). Unlike A53T, tubular particles were not observed for A30P. The possibility that the tubular particles of A30P did not adsorb to the EM grids is unlikely, since they were clearly present in samples of A53T. These results are consistent with the narrow molecular mass distribution predicted by SVAU and the reduced assembly rate of A30P relative to A53T.

Discussion

The two PD-linked mutations A30P and A53T promote the formation of α-synuclein protofibrils, suggesting a causal role for protofibril formation in PD.[11,13,16] These protofibrillar intermediates are structurally heterogeneous. To identify a pathogenic protofibrillar species and to understand the relationship between their morphologies and cytotoxicity requires a detailed characterization of the protofibrils. Here, we apply negative stain EM and single-particle averaging to characterize the formation and structural heterogeneity of α-synuclein protofibrils by WT α-synuclein and the PD-linked variants A30P and A53T. To facilitate the structural characterization of protofibrils, GF, SVAU, and STEM were utilized in parallel with EM to obtain protofibrillar preparations of defined molecular size distribution and morphology. Several important themes have emerged from this work.

Parkinson's disease-linked mutations promote the formation and/or stabilize annular α-synuclein protofibrils

Despite the heterogeneity of the protofibrils, SVAU analysis revealed that all three α-synuclein variants populated predominantly three major classes, with sedimentation coefficients of 13 S, 17 S, and 25 S, suggesting common fibrillization intermediates. It is important to emphasize that neither the 13 S nor 17 S species corresponds to a single sedimenting protofibrillar species, but rather to a narrow distribution of protofibrils with an average sedimentation coefficient of 13 S or 17 S. The A53T mutation, in addition to promoting protofibril formation,[13] shifted the molecular size distribution towards higher M_r protofibrils relative to the WT and A30P variants. These three classes of protofibrils were purified partially by GF. Characterization of these fractions by EM, image processing and STEM revealed novel annular and tubular protofibrillar structures, in addition to the previously reported spherical and chain-like morphologies. The annular protofibrils had an average diameter of 11(±1) nm, and an inner diameter of 2–3 nm; the tubular protofibrils showed similar diameter (10–12 nm), and varied in length from 12 nm to 24 nm.

Molecular masses estimated from the sedimentation coefficient and obtained from STEM analysis suggest that the smallest oligomeric species has $M_r \sim 140$ kDa, pointing to a decamer as the smallest detectable metastable oligomer. Both techniques also suggest an average M_r of ~350(±50) kDa for the annular protofibrils. Each of the techniques used for the determination of M_r has its own limitations. GF depends on the shape of the protein and its interaction with the column matrix, whereas estimates on the basis of the sedimentation coefficient values assume a globular structure for all protofibrils which is not the case in all samples. STEM measurements are on the basis of the assumption that all protofibrillar species were equally adsorbed on the surface of the EM grid. We have addressed these issues by comparing the results from three complementary approaches (AU, STEM, and GF), allowing the size of the protofibrils to be estimated with a good degree of accuracy.

EM images showed that the protofibrils formed by both A53T and A30P variants populated three or four morphological classes, the most common type being the annular protofibrils. Although both variants rapidly formed annular structures, tubular protofibrils were observed only for A53T. In contrast to the PD-linked variants, WT α-synuclein

formed annular protofibrils only after incubation for several (six to eight) weeks. A wide range of bacterial and insect toxins utilize α-helices to perturb or penetrate membranes, whereas other toxins, such as aerolysin and staphylococcal α-hemolysin, form β-barrels that span the membrane.[20,21] Formation of β-barrels lowers the energetic barrier for the insertion of non-hydrogen-bonded β-strands into the membranes. Generally, these β-barrels are composed of 8–22 β-strands (ten to 13 residues) and have an average diameter of 1.5–3.5 nm.[21,22] In α-hemolysin (heptamer), each monomer contributes an amphipathic hairpin to a 14-stranded β-barrel.[23] α-Synuclein annular protofibrils have secondary (β-sheet) and quaternary (2.5 nm pore-like annular and tubular structures) structural features in common with aerolysin and staphylococcal α-hemolysin. The data presented here do not prove that α-synuclein self-assembles to a β-barrel pore. However, on the basis of our observations, we speculate that a β-strand solvent-accessible pore with a diameter of 2–3 nm could be formed by β-barrel structures composed of 20–24 α-synuclein monomers.

The different protofibrillar morphologies seem to be related

A relationship between spherical and annular protofibrils has been proposed on the basis of AFM studies of α-synuclein.[17] The studies above do not address the pathway, but the intermediates may represent protofibrils at different assembly stages in a linear or parallel path to the stable fibrils. Annular and tubular protofibrils have similar diameters, suggesting that the two structures represent the two different views (top and side-view) of the same protofibrillar species, with their different appearance in electron micrographs merely reflecting different interactions with the surface of the carbon-coated copper grid. Incubation of samples rich in annular protofibrils at 4 °C (four to eight weeks) revealed images with an increasing population of longer tubes, a result that could also be caused by an increasing propensity of tubes to adsorb with their sides to the grid as they grow in length. This transition coincides with a shift in the molecular size distribution of the protofibrils from 13 S (predominately annular) to 17(±1) S (predominately tubular).

α-Synuclein protofibrils are precursors to fibrils, but the mechanism of conversion remains unknown

In the presence of monomeric α-synuclein, annular and tubular protofibrils were consumed upon fibril formation, consistent with their being transient assembly intermediates on the fibril formation pathway. The fibrils exhibited a helical twist and have a diameter that is similar to that of the annular and tubular protofibrils (ca 11 nm). Although a model in which the amyloid fibril is a hollow cylinder or tube has been proposed on the basis of the X-ray fiber diffraction data,[24,25,47] the resolution of the EM data presented here does not allow conclusions to be drawn about whether this is the case for α-synuclein fibrils. The mechanism by which annular and tubular protofibrils convert to fibrils is under investigation in our laboratory. Both annular and tubular protofibrils, like the fibrils, showed β-sheet secondary structure and resistance to proteolysis by PK.[18] Together, these results indicate that the inter-monomer interactions in the protofibril are similar to those of the fibril, suggesting a common core structure.

The annular, pore-like protofibrils may be responsible for *in vitro* vesicle permeabilization and, possibly, PD

Although a toxic role for protofibrils has been suggested in several neurodegenerative diseases, the mechanism of its toxicity has not been elucidated.[14,26–28] Our own studies have demonstrated that protofibrillar α-synuclein exhibits tight binding to phosphatidylglycerol (PG) vesicles *via* a β-sheet-rich oligomeric structure, and binding results in permeabilization. Monomeric and fibrillar α-synuclein showed little binding and no permeabilization activity.[19] Size-dependent permeabilization studies revealed that small (calcium, dopamine and fura-2) molecules were released from the vesicles by α-synuclein protofibrils, whereas large molecules such as FITC-dextran (4400, 26 Å in diameter) were impermeable.[29] These results suggest that vesicle permeabilization may occur largely as a result of a specific membrane perturbation, likely *via* the formation of a pore that is at least 2.5 nm in diameter, consistent with the diameter of the annular and tubular protofibrils described here. Addition of protofibrillar α-synuclein (WT or A53T) to brain-derived vesicle (BDV) fractions allowed the observation of pore-like structures,[17] which resemble, in overall morphology and dimension, membrane-spanning pores that are formed by protein toxins (e.g. hemolysin, latrotoxin, and aerolysin).[20,30] In preliminary experiments, the annular and tubular protofibril fractions were observed to permeabilize synthetic vesicles (M. Volles & H.A.L., unpublished results), providing further support for the conclusion that permeabilization by α-synuclein protofibrils occurs *via* a localized pore-like mechanism.[29] Several amyloidogenic proteins associated with different neurodegenerative diseases (Alzheimer's disease, Huntington disease, and prion diseases) form ion-permeable pores at cytotoxic concentrations, strongly suggesting that membrane disruption, *via* pore formation, may be a general mechanism of cytotoxicity for neurodegenerative diseases.[19,29,31–36]

We propose that an increase in the levels of protofibrils or the selective population of particular protofibrillar morphologies may initiate early PD. Several factors are likely to modulate the formation and stability of α-synuclein protofibrils *in vivo*,

including mutations, post-translational modifications and interactions with related proteins. For example, the interaction of α-synuclein with dopamine promotes the formation of protofibrils.[37] Finally, a significant implication of our findings is that there may be a close relationship between formation of pore-like protofibrils, membrane permeabilization and the mechanism of neurotoxicity in PD.

Materials and Methods

Preparation and purification of α-synuclein protofibrils

Recombinant α-synuclein was expressed and purified as described.[13] To prepare α-synuclein protofibrils, lyophilized α-synuclein variants were dissolved in phosphate-buffered saline (PBS) (0.01 M sodium phosphate buffer (pH 7.4), 150 mM NaCl) to obtain concentrations of 300–700 μM. The stock solutions were incubated on ice for 30–60 minutes before being centrifuged at 16,000*g* for five minutes, and filtered through a 0.22 μm nylon spin filter (Costar) to remove any insoluble particles. The filtrates were loaded (100 μl/injection) onto a Superdex 200 HR (Amersham Pharmacia) GF column equilibrated with protein buffer (10 mM Tris–HCl (pH 7.4), 150 mM NaCl), and protein was eluted at a flow-rate of 0.5 ml/minute. Fractions of 0.5 ml were collected using a Waters fraction collector (model II). Fractions corresponding to the void peak were either combined or split into three fractions (early, middle, and late) and used for biophysical studies. Purified protofibril fractions were stored at 4 °C. Samples for EM and SVAU were prepared within three days unless indicated otherwise.

Molecular mass determination using GF

α-Synuclein samples (300 μM) in volumes of 100–150 μl were injected onto the column (Superdex 200 or Tsk-Gel G4000 SWxl) and eluted at a flow-rate of 0.5 ml/minute. The retention time for the protein was monitored by measuring the absorbance at 220 nm, 254 nm, and 280 nm. The M_r value for the α-synuclein samples was estimated using the following standards: blue dextran, 2000 kDa; thyroglobulin, 669 kDa; ferritin, 440 kDa; catalase, 232 kDa; aldolase, 158 kDa; albumin, 68 kDa; chymotrypsinogen A, 25 kDa; and ribonuclease A, 13.7 kDa.

Circular dichroism spectroscopy

Far-UV CD spectra of purified protofibrils in protein buffer (10 mM Tris–HCl (pH 7.4), 150 mM NaCl) were collected at 25 °C using an Aviv 62A DS spectrophotometer and a 0.1 cm cuvette. Data were acquired at a step size of 0.2 nm with an averaging time of three seconds. For each sample, the mean residue ellipticity was reported as an average of three scans.[38]

Electron microscopy and image processing

Purified protofibril fractions of A53T and A30P α-synuclein were diluted sixfold with protein buffer prior to adsorption to glow-discharged, carbon-coated copper grids. Grids were washed with four drops of buffer and stained with two drops of freshly prepared 0.75% (w/v) uranyl formate (Pfaltz & Bauer, Waterbury, CT 06708). Specimens were inspected with a Philips Tecnai 12 electron microscope operated at 120 kV and images were taken at a nominal magnification of 52,000 × using low-dose procedures. For image processing, 31 images of A53T (late fraction of the void peak) and 16 images of A30P (middle fraction of the void peak) were digitized with a Zeiss SCAI scanner using a pixel size of 4.04 Å at the specimen level. From the digitized images, 5815 (A53T), and 5040 (A30P) particles were selected for further computational processing using the SPIDER image processing package.[39] The 5000–6000 particle images were subjected to ten rounds of alignment and classification specifying 100 output classes. In the case of α-synuclein fibrils, 1172 fibril crossovers were cut out from 30 images, from which 549 were included in the final projection average.

Sedimentation velocity analytical ultracentrifugation (SVAU)

Sedimentation velocity data were collected in a temperature-controlled Beckman XL-A. A double-sector cell, equipped with a 12 mm Epon centerpiece and quartz windows was loaded with 400–420 μl of protein sample. Data were collected at rotor speeds of 3000–60,000 rpm in continuous mode at 25 °C, with a step size of 0.005 cm and an average of three scans per point. Purified void fractions isolated by GF and stored at 4 °C were incubated at room temperature for one to two hours prior to the SVAU experiments at 25 °C.

Analysis of the sedimentation velocity data

For samples containing α-synuclein monomer or a monomer–dimer mixture, the absorbance data were fit using the direct boundary fitting approach using the Svedberg analysis program developed by Philo as described.[40] For heterogeneous samples containing multiple species, the sedimentation velocity absorbance profiles were analyzed to obtain the apparent distribution of sedimentation coefficients $g(s^*)$ for all the quaternary structures in solution using the DCDT software provided by Philo.[41,42] The M_r value of globular proteins can be estimated from their sedimentation coefficient using equation (1), where $\bar{\upsilon}$ is the partial specific volume of α-synuclein (ml/g), and ρ is the density of the solvent (in g/ml).[43] The partial specific volume of α-synuclein (0.734 cm^3/g) was estimated on the basis of the partial specific volumes of the component amino acid residues, whereas the density of the buffers was calculated using polynomial equations and tables of coefficients solution:[44,45]

$$(M_r)^{\frac{2}{3}} = \frac{100 s \bar{\upsilon}^{\frac{1}{3}}}{(1 - \bar{\upsilon}\rho)} \quad (1)$$

Scanning transmission electron microscopy (STEM)

Protofibril fractions of A53T and A30P were analyzed by STEM at the Brookhaven National Laboratory using unstained, freeze-dried samples. Protein samples (10–20 μM) were applied to a thin carbon film supported by a thick holey film on titanium grids, wicked to a thin layer, frozen rapidly to avoid ice crystal formation and freeze-dried overnight. The freeze-dried, unstained

specimens were transferred to the STEM under vacuum and examined at −150 °C and 40 kV using the annular dark-field detector mode. Tobacco mosaic virus (TMV) was included in all specimens to monitor preparation quality. Digital images of 512 × 512 pixels with 1 nm spacing were recorded at an average dose of 300–1000 e/nm^2. Processing of the STEM data for mass determination was carried out using the PCMass software package as described.[46]

Digestion with proteinase K (PK)

A 1 μl aliquot of 150 μg/μl of proteinase K (Sigma) was added to 35 μl of purified A53T (late fraction) protofibrils. Before addition of PK, 10 μl of a protofibril solution was boiled in SDS running buffer and incubated at room temperature for four hours to serve as a control for the untreated sample. At different time-points, an aliquot of 10 μl was taken for analysis. Each aliquot was quenched by addition of SDS sample buffer and boiled for ten minutes before being resolved on an SDS/10–20% (w/v) polyacrylamide gel (tricine (*N*-[Tris-hydroxymethylo-methyl]-glycine) buffer). The proteins were detected by silver staining.

Acknowledgments

We thank Yichin Liu, Mike Volles, and Dean Hartley for insightful discussions and for critical review of the manuscript. This work was supported by a Morris K. Udall Parkinson's Disease Research Center of Excellence grant (NS38375), the James K. Warsaw Foundation to Cure Parkinson's Disease, and the Kinetics Foundation. H.A.L. is a postdoctoral fellow of the Laboratory for Drug Discovery in Neurodegeneration, a core component of the Harvard Center for Neurodegeneration and Repair. The molecular EM facility at Harvard Medical School was established by a generous donation from the Giovanni Armenise Harvard Center for Structural Biology and is maintained by funds from NIH grant GM62580. The BNL STEM is an NIH Supported Resource Center, NIH P41-RR01777, with additional support provided by DOE, OBER.

References

1. Pollanen, M. S., Dickson, D. W. & Bergeron, C. (1993). Pathology and biology of the Lewy body. *J. Neuropathol. Expt. Neurol.* **52**, 183–191.
2. Forno, L. S. (1996). Neuropathology of Parkinson's disease. *J. Neuropathol. Expt. Neurol.* **55**, 259–272.
3. Dunnett, S. B. & Bjorklund, A. (1999). Prospects for new restorative and neuroprotective treatments in Parkinson's disease. *Nature*, **399**, A32–A39.
4. Spillantini, M. G., Crowther, R. A., Jakes, R., Hasegawa, M. & Goedert, M. (1998). alpha-Synuclein in filamentous inclusions of Lewy bodies from Parkinson's disease and dementia with lewy bodies. *Proc. Natl Acad. Sci. USA*, **95**, 6469–6473.
5. Polymeropoulos, M. H., Lavedan, C., Leroy, E., Ide, S. E., Dehejia, A., Dutra, A. *et al.* (1997). Mutation in the alpha-synuclein gene identified in families with Parkinson's disease. *Science*, **276**, 2045–2047.
6. Kruger, R., Kuhn, W., Muller, T., Woitalla, D., Graeber, M., Kosel, S. *et al.* (1998). Ala30Pro mutation in the gene encoding alpha-synuclein in Parkinson's disease. *Nature Genet.* **18**, 106–108.
7. Masliah, E., Rockenstein, E., Veinbergs, I., Mallory, M., Hashimoto, M., Takeda, A. *et al.* (2000). Dopaminergic loss and inclusion body formation in alpha-synuclein mice: implications for neurodegenerative disorders. *Science*, **287**, 1265–1269.
8. Feany, M. B. & Bender, W. W. (2000). A Drosophila model of Parkinson's disease. *Nature*, **404**, 394–398.
9. Conway, K. A., Harper, J. D. & Lansbury, P. T. (1998). Accelerated *in vitro* fibril formation by a mutant alpha-synuclein linked to early-onset Parkinson disease. *Nature Med.* **4**, 1318–1320.
10. Conway, K. A., Lee, S. J., Rochet, J. C., Ding, T. T., Harper, J. D., Williamson, R. E. & Lansbury, P. T., Jr (2000). Accelerated oligomerization by Parkinson's disease linked alpha-synuclein mutants. *Ann. NY Acad. Sci.* **920**, 42–45.
11. Rochet, J. C., Conway, K. A. & Lansbury, P. T., Jr (2000). Inhibition of fibrillization and accumulation of prefibrillar oligomers in mixtures of human and mouse alpha-synuclein. *Biochemistry*, **39**, 10619–10626.
12. Li, J., Uversky, V. N. & Fink, A. L. (2001). Effect of familial Parkinson's disease point mutations A30P and A53T on the structural properties, aggregation, and fibrillation of human alpha-synuclein. *Biochemistry*, **40**, 11604–11613.
13. Conway, K. A., Lee, S. J., Rochet, J. C., Ding, T. T., Williamson, R. E. & Lansbury, P. T., Jr (2000). Acceleration of oligomerization, not fibrillization, is a shared property of both alpha-synuclein mutations linked to early-onset Parkinson's disease: implications for pathogenesis and therapy. *Proc. Natl Acad. Sci. USA*, **97**, 571–576.
14. Goldberg, M. S. & Lansbury, P. T., Jr (2000). Is there a cause-and-effect relationship between alpha-synuclein fibrillization and Parkinson's disease? *Nature Cell Biol.* **2**, E115–E119.
15. Tompkins, M. M., Basgall, E. J., Zamrini, E. & Hill, W. D. (1997). Apoptotic-like changes in Lewy-body-associated disorders and normal aging in substantia nigral neurons. *Am. J. Pathol.* **150**, 119–131.
16. Conway, K. A., Harper, J. D. & Lansbury, P. T., Jr (2000). Fibrils formed *in vitro* from alpha-synuclein and two mutant forms linked to Parkinson's disease are typical amyloid. *Biochemistry*, **39**, 2552–2563.
17. Ding, T. M., Lee, S-J., Rochet, C. J. & Lansbury, P. T., Jr (2002). Annular a-synuclein protofibrils are produced by spherical protofibrils incubated in solution or bound to membrane surfaces. *Biochemistry*, **41**, 10209–10217.
18. Giasson, B. I., Murray, I. V., Trojanowski, J. Q. & Lee, V. M. (2001). A hydrophobic stretch of 12 amino acid residues in the middle of alpha-synuclein is essential for filament assembly. *J. Biol. Chem.* **276**, 2380–2386.
19. Volles, M. J., Lee, S. J., Rochet, J. C., Shtilerman, M. D., Ding, T. T., Kessler, J. C. & Lansbury, P. T., Jr (2001). Vesicle permeabilization by protofibrillar alpha-synuclein: implications for the pathogenesis and treatment of Parkinson's disease. *Biochemistry*, **40**, 7812–7819.
20. Valeva, A., Palmer, M. & Bhakdi, S. (1997). Staphylococcal alpha-toxin: formation of the heptameric pore is partially cooperative and proceeds through multiple intermediate stages. *Biochemistry*, **36**, 13298–13304.

21. Heuck, A. P., Tweten, R. K. & Johnson, A. E. (2001). B-Barrel pore-forming toxins: intriguing dimorphic proteins. *Biochemistry*, **40**, 9065–9073.
22. Heuck, A. P., Hotze, E. M., Tweten, R. K. & Johnson, A. E. (2000). Mechanism of membrane insertion of a multimeric beta-barrel protein. Perfringolysin O creates a pore using ordered and coupled conformational changes. *Mol. Cell*, **6**, 1233–1242.
23. Menestrina, G., Serra, M. D. & Prevost, G. (2001). Mode of action of beta-barrel pore-forming toxins of the staphylococcal alpha-hemolysin family. *Toxicon*, **39**, 1661–1672.
24. Malinchik, S. B., Inouye, H., Szumowski, K. E. & Kirschner, D. A. (1998). Structural analysis of Alzheimer's beta(1–40) amyloid: protofilament assembly of tubular fibrils. *Biophys. J.* **74**, 537–545.
25. Serpell, L. C., Blake, C. C. & Fraser, P. E. (2000). Molecular structure of a fibrillar Alzheimer's A beta fragment. *Biochemistry*, **39**, 13269–13275.
26. Rochet, J. C. & Lansbury, P. T., Jr (2000). Amyloid fibrillogenesis: themes and variations. *Curr. Opin. Struct. Biol.* **10**, 60–68.
27. Haass, C. & Steiner, H. (2001). Protofibrils, the unifying toxic molecule of neurodegenerative disorders? *Nature Neurosci.* **4**, 859–860.
28. El-Agnaf, O. M., Nagala, S., Patel, B. P. & Austen, B. M. (2001). Non-fibrillar oligomeric species of the amyloid ABri peptide, implicated in familial British dementia, are more potent at inducing apoptotic cell death than protofibrils or mature fibrils. *J. Mol. Biol.* **310**, 157–168.
29. Volles, M. J. & Lansbury, P. T., Jr. (2002). Vesicle permeabilization by protofibrillar a-synuclein: comparison of wild-type with parkinson's disease linked mutants and insights in the mechanism. *Biochemistry*, **41**, 4595–4602.
30. Parker, M. W., van der Goot, F. G. & Buckley, J. T. (1996). Aerolysin–the ins and outs of a model channel-forming toxin. *Mol. Microbiol.* **19**, 205–212.
31. Kawahara, M. & Kuroda, Y. (2000). Molecular mechanism of neurodegeneration induced by Alzheimer's beta-amyloid protein: channel formation and disruption of calcium homeostasis. *Brain Res. Bull.* **53**, 389–397.
32. Hirakura, Y. & Kagan, B. L. (2001). Pore formation by beta-2-microglobulin: a mechanism for the pathogenesis of dialysis associated amyloidosis. *Amyloid*, **8**, 94–100.
33. Kourie, J. I., Henry, C. L. & Farrelly, P. (2001). Diversity of amyloid beta protein fragment [1-40]-formed channels. *Cell. Mol. Neurobiol.* **21**, 255–284.
34. Pillot, T., Drouet, B., Pincon-Ramond, M., Vandekerckhove, J., Rosseneu, M. & Chambaz, J. (2000). A nonfibrillar form of the fusogenic prion protein fragment [118-135] induces apoptotic cell death in rat cortical neurons. *J. Neurochem.* **75**, 2298–2308.
35. Lin, H., Bhatia, R. & Lal, R. (2001). Amyloid beta protein forms ion channels: implications for Alzheimer's disease pathophysiology. *FASEB J.* **15**, 2433–2444.
36. Mirzabekov, T. A., Lin, M. C. & Kagan, B. L. (1996). Pore formation by the cytotoxic islet amyloid peptide amylin. *J. Biol. Chem.* **271**, 1988–1992.
37. Conway, K. A., Rochet, J. C., Bieganski, R. M. & Lansbury, P. T., Jr (2001). Kinetic stabilization of the alpha-synuclein protofibril by a dopamine-alpha-synuclein adduct. *Science*, **294**, 1346–1349.
38. Schmid, F. X. (1989). *Protein Structure: A Practical Approach* (Creighton, T. E., ed.), pp. 251–285, IRL Press, New York.
39. Frank, J., Radermacher, M., Penczek, P., Zhu, J., Li, Y., Ladjadj, M. & Leith, A. (1996). SPIDER and WEB: processing and visualization of images in 3D electron microscopy and related fields. *J. Struct. Biol.* **116**, 190–199.
40. Philo, S. J. (1994). Measuring sedimentation, diffusion, and molecular weights of small molecules by direct fitting of sedimentation velocity concentration profiles. In Modern Analytical Ultracentrifugation (Shuster, T. M. & Laue, T. M., eds), pp. 156–170, Springer-Verlag, Heidelberg.
41. Philo, J. S. (1997). An improved function for fitting sedimentation velocity data for low-molecular-weight solutes. *Biophys. J.* **72**, 435–444.
42. Stafford, W. F., III (1994). Boundary analysis in sedimentation velocity experiments. *Methods Enzymol.* **240**, 478–501.
43. Lashuel, H. A., Lai, Z. & Kelly, J. W. (1998). Characterization of the transthyretin acid denaturation pathways by analytical ultracentrifugation: implications for wild-type, V30M, and L55P amyloid fibril formation. *Biochemistry*, **37**, 17851–17864.
44. Durchschlag, H. (1986). Specific volumes of biological macromolecules and some other molecules of biological interest. In *Thermodynamic Data for Biochemistry and Biotechnology* (Hinz, H.-J., ed.), pp. 45, Springer, New York.
45. Perkins, S. J. (1986). Protein volumes and hydration effects. The calculations of partial specific volumes, neutron scattering matchpoints and 280-nm absorption coefficients for proteins and glycoproteins from amino acid sequences. *Eur. J. Biochem.* **157**, 169.
46. Wall, J. S. & Simon, M. N. (2001). Scanning transmission electron microscopy of DNA–protein complexes. *Methods Mol. Biol.* **148**, 589–601.
47. Perutz, M. F., Finch, J. T., Berriman, J. & Lesk, A. Amyloid fibers are water-filled nanotubes. *Proc. Natl. Acad. Sci. USA*, **99**, 5591–5595.

Edited by F. E. Cohen

(Received 23 May 2002; received in revised form 2 July 2002; accepted 10 July 2002)

http://www.academicpress.com/jmb

Supplementary Material comprising six Figures is available on IDEAL

Note added in proof: After submission of this manuscript, we learned that we can obtain a better separation of A53T α-synuclein protofibrils by using a Superose 6 GF column (10/30 HR Amersham Pharmacia) instead of a Superdex 200 (10/30 HR Amersham Pharmacia). Usage of this column yielded a more homogeneous protofibri distribution, especially for the lowest M_r fraction (Late) as was verified by EM (Supplementary Figure 5) and STEM (Supplementary Figure 6).